

Numerical Modeling and Laboratory study of Layered Gypsum-Concrete Specimens with Joints

Alireza Bagher Shemirani^{1*}

¹ Faculty of Civil, Water & Environmental Engineering, Shahid Beheshti University, Tehran, Iran

* Corresponding author: a_baghershmirani@sbu.ac.ir

Corresponding Author: Tel:+98-9122473788

Abstract

The existence of joints and defects around the openings causes the instability of these flaws. In nature, rocks or concrete materials are layered and anisotropic and have many joints. Therefore, in this article, the layered gypsum-concrete specimens were created and examined in the laboratory with different geometries, and the single joint above the opening with different angles. The instability and specimen failure were studied about the angularity of joints, anisotropy, and the opening's geometry.

Also, the numerical modeling of the tested specimen is done with ABAQUS software to study the behavior of the opening during interaction with a joint or fault. The ABAQUS software was calibrated by using a uniaxial compression test. Then, the modeled specimens are presented so that different opening configurations with joints are tested under uniaxial compression conditions. This study showed that tensile cracks are the most dominant mode in these modeled specimens. As the connection distance from the tunnel roof increases, its effect on tunnel instability decreases because the failure stress increases.

Keywords: Crack, opening, layered gypsum-concrete specimens, joint, ABAQUS

Introduction:

Tunnels are dug inside rock masses containing seams, fractures, bed plates, and other excavation defects. The presence of joints and faults affects the mechanical behavior of the rocks around openings. Stability and safety of tunnels in layered and jointed rocks are important to design engineers [1, 2]. When the joint and faults cut off the tunnel, it can be the most dangerous tunnel situation inside the rock, which requires careful design to prevent structural instability. Some experimental and numerical studies have been performed on concrete specimens, including samples with pre-existing cracks of different orientations, to evaluate crack propagation. These investigations showed that the presence of cracks weakens the mechanical properties of these materials, leading to sample destruction and instability [3-14].

Li et al. [15] analyzed large deformations in openings within high-stress areas. They discussed the factors influencing deformation and failure models and suggested optimal construction timing for lining. Sun et al. [16] conducted an analyzed the instability present in jointed rock masses within openings through both experimental and numerical modeling techniques. They demonstrated that pre-stressed rock bolts can control deformation within a range of 2-5 mm, thereby improving the measure of the ultimate load of rock mass in joint openings.

Si et al. [17] have done triaxial experiments on sand specimens featuring a "D" shaped hole to understand their failure characteristics. They compared the cracks patterns of the two rock models and attributed the differences to variations in clay mineral amount and the existence of

weak bedding layers. Deng et al. [18] conducted a study using a split Hopkinson pressure bar apparatus to study how orientation of dynamic loading impacts twin-tunnel stability during blasting excavation. They found that the angle of dynamic loading have a brilliant influence on crack beginning and stress distribution. Chen et al. [19] studied fracture mechanisms in deep-jointed soft-rock openings. They observed complex deformation patterns and the effectiveness of active control methods such as pre-stressed support and grouting for stability. Li et al. [20] investigated filled structural planes in brittle rock masses. The impacts of dip inclination and infill height on breakage modes are remarkable. Huang et al. [21] conducted triaxial tests and numerical simulations to investigate the anisotropy of layered shale samples on shear, slip, and combined failure modes.

Chen and Teng [22] conducted several 3DEC models to investigate stratified rock openings. They found that the arrangement of secondary flaws in rock masses and fractured areas may affect bedding planes. He et al. [23] investigated crack orientation effects with different orientation angles using rock bursts in deep openings. They determined the breakage paths in the surrounding rock mass. Some researchers studied the influence of pre-existing inclinations, arrangements, and failure processes in rock specimens.

The innovative advances achieved over previous work can be demonstrated by integrating the current research with the existing literature. Zhou and Yang [24] present a multi-scale numerical model used the extended finite element method (XFEM) to pretend damage progression in crack-affected rock masses. Their method effectively captures the dynamics of multiple crack formations without requiring re-meshing, providing valuable insights into crack growth and merging in heterogeneous materials. Meanwhile, Chen et al. [25] focus on the behavior of rock masses, highlighting critical influence of weak interlayers and fractures under dynamic loading conditions. While both studies contribute valuable findings regarding crack behavior and the impact of internal discontinuities, the article introduces a novel approach to the creation of seams over openers. This study examines various seam placements and the effects of different opener shapes, aspects that have not been previously addressed. By considering the anisotropic model of the plaster-concrete sample, it examines the innovative notion of placing joints specifically in weak layers directly atop the opener. This distinct focus on seam creation and its interaction with opener shapes marks a significant progression in the understanding of the mechanics of rock masses when influenced by anisotropy. The findings not only fill a notable gap in the existing literature but also expand the foundational knowledge necessary for safe engineering practices, thereby reflecting a substantial scientific advancement in the study of rock mechanics.

Chen and Zhou [26] explored the impact of crack length and wavelength on cracking by utilizing the extended finite element method (XFEM) with an absorbing boundary condition. Their findings indicated that the angle of dynamic loads relative to cracks greatly affects energy dynamics, while crack length has a minimal effect. They found that wavelengths shorter than a critical threshold led to tensile-shear cracking, while longer wavelengths resulted in compression-shear and tension-shear behaviors. Zhou and Jia [27] proposed an area-enhanced finite element model to analyze the crack extension in fragile materials, validating it against stress intensity factors in crack propagation, effectively replicating various experimental results. They also examined how circular holes affect the paths of existing cracks. Chen et al. [28] introduced an improved method that enhances the degree of freedom for absorbing outgoing elastic waves in elastodynamic problems. Their approach utilizes a mass matrix that gradually increases, which helps improve wave damping. This method has proven effective in various scenarios, including cases with multiple cracks. The study emphasized that it is adaptable for

both field-scale and laboratory-scale applications. Zhou et al. [29] created a novel method to model frictional contact issues. By integrating Coulomb's friction model, they addressed the issue of stress redistribution at crack surfaces and successfully mitigated locking phenomena in their simulations. Their results showcased the method's precision and efficiency in dealing with frictional contact challenges in crack-related problems. Chen et al. [30] focused on modeling crack propagation with XFEM and hierarchical mesh adaptation. They showed which crack tip stresses will be accurately closed using stress intensity coefficients and T-stress terms, ensuring high accuracy through least squares fitting.

Zhou et al. [31] performed compressive experiments on granite specimens containing flaws, using digital imaging and acoustic emission methods for real-time observation. They proposed a unique technique for analyzing acoustic emission (AE) data through the inter-event time function and categorized cracking events into six levels based on five distinct stress values. For the first time, they illustrated the formation of process zones and found connections with strain fields. In another investigation, Zhou et al. [32] studied rock-like materials with various flaws subjected to uniaxial compression. They classified five different crack types and identified ten coalescence scenarios, evaluating how the arrangement of flaws influences mechanical behavior. In the meantime, Chen and Zhou [33] improved the XFEM for the complex propagation of branched cracks. Their method, which utilizes a variable length for crack propagation, showed enhanced precision and produced smoother crack trajectories compared to conventional XFEM. Chen et al. [34] focused on modeling crack propagation with XFEM and hierarchical mesh adaptation. They showed that crack tip stresses can be accurately approximated using stress intensity factors and T-stress terms, ensuring high accuracy through least squares fitting.

In this article, it focuses on joints placed above openings and the types of seams and shapes involved. The analysis of a plaster-concrete sample suggests placing joints in weak layers above the opening. This view fills a gap in current research and helps understand rock mass mechanics affected by anisotropy. The research shows the effects of anisotropy and opening geometry on instability and failure in layered concrete gypsum specimens with different geometries. It examines a single joint above the opening at different angles through experiments and numerical analysis.

Experimental Studies

In this study, two material models were utilized to evaluate the effect of anisotropy and joints on the breakage mechanism of layered concrete samples under compression test. The first referred to as material A, was comprised of concrete with a cement-to-water ratio of 2.5:1 (by weight). The second referred to as material B, was composed of gypsum.

The necessary number of concrete samples was created in the lab using combinations of Portland cement, water, silica fume, aggregates (sand and gravel), and superplasticizers. The behaviors of cement and silica fume can be found in Table 1, while the characteristics of the aggregates are listed in Table 2. An overview of the concrete specimen mix designs can be found in Table 3.

For the creation of specimens containing gypsum, a mixture of gypsum and water in a 2:1 aspect was poured into the molds.

The mold has the dimensions of 200 mm × 200 mm × 60 mm. The framework is made of fiberglass. A sponge was placed inside the frame to create a hole (as a tunnel). A thin plastic sheet was used between the two layers. Also, aluminum sheets with dimensions of 1 mm × 20 mm × 100 mm were used to create a seam above the cavity.

Initially, a plaster layer measuring 60 mm × 200 mm × 100 mm was made. Right after, a sponge was inserted in the plaster to create a hole, while an aluminum sheet was placed on top of the

hole to form a seam. After 15 minutes, once the plaster dried, the oil-soaked sheet was taken out. Subsequently, a concrete section measuring 100 mm × 200 mm × 60 mm was created. Then, the mold screws were loosened, and the specimens were taken out. After 28 days, the specimens were subjected to compressive loading to study their mode of failure.

The mechanical characteristics of the gypsum and concrete are displayed in Tables 4 and 5, respectively. To create gypsum-concrete samples, boxes by the dimensions of 200 mm × 200 mm × 60 mm be built, and two rectangular spaces (gypsum placed on concrete) were located on one face (Fig. 1). To form the concrete and gypsum layers, grout and gypsum were poured into a custom-designed wooden container, as shown in Fig. 2. Subsequently, these specimens were tested using a uniaxial test apparatus at a loading rate of 0.001 mm/sec, as illustrated in Fig. 3.

It considers only uniaxial compression for simplicity and focus in the analysis. This type of loading allows for a clear understanding of the material behavior under straightforward conditions, making it easier to isolate variables and interpret results. Additionally, uniaxial compression is a common loading scenario in many practical applications, and studying it provides valuable insights into the failure mechanisms. Future work may also include other loading types, such as biaxial or triaxial tests, to provide a more comprehensive view of material performance under varied conditions. It chooses to focus exclusively on uniaxial compression for several reasons. Firstly, uniaxial compression simplifies the analysis by allowing for a clear understanding of the material behavior under a single, controlled loading condition. This uniformity aids in isolating key variables and makes interpreting results more straightforward. Also, uniaxial loading is important in many practical applications, especially concerning tunnels and rock formations, where materials typically endure similar compressive stresses. Concentrating on this loading scenario, it gains important insights into failure mechanisms that are crucial for understanding material behavior in practical applications. Additionally, starting with uniaxial compression establishes a fundamental step in material testing. Once a thorough understanding is established, future research can build upon these findings by exploring more complex loading conditions like biaxial or triaxial tests. This sequenced approach allows for incremental learning and a more comprehensive understanding of material performance under varying conditions.

In this study, experiments are performed on specially prepared rectangular specimens measuring 200 mm × 200 mm × 60 mm. Six rectangular specimens were fabricated from two layers of concrete and gypsum with a joint. To create the tunnel and joint, a thin plate and an opening mold were pre-inserted into a rectangular mold and then removed after the initial hardening of the specimen. The joints with different angles and different openings are illustrated in Figs. 4 (a-f), respectively. These joints' geometries are characterized by parameter α to express the inclination angles of joints. The experimental system included the test bed, control system, and data logger. Figs 5a to 1f display the fabricated specimens from the two concrete-gypsum layers with a joint.

Failure pattern of experimental test

The experimental failure patterns obtained for specimens of concrete-gypsum layers with openings containing a single joint under uniaxial compressive test are presented (Fig. 6).

When a notch (joint or fault) is positioned at a 45° angle from the top of the tunnel, as shown in Fig. 6a, it indicates that the joint or fault interrupts the tunnel. In this case, a wing crack begins at the tip of the joint and spreads aligned to the force axis, while a secondary crack develops near

the surface. Instability in the tunnel walls (opener) occurs before failure reaches the rupture surface. The rupture surface represents a critical transition zone where the structural integrity of the material is compromised, leading to separation or fracture. Understanding this concept is essential in material science, as it provides insights into failure mechanisms and material behavior under stress. In Fig. 6b, when the joint is positioned vertically (at a 90-degree angle) at the top of the tunnel, effectively interrupting it, cracking begins at the tip of the fissure and transmits diagonally toward the surface of sample. Before the tunnel walls collapse, the sample becomes torn from the joint due to the advancing crack. In Fig. 6c, the joint is located above the opening at an angle of 125°, which does not interrupt the tunnel. Here, a wing (tensile) crack may initiate from either side of the joint tip and interact with the specimen surface, extending from the lower tip toward the opening and from the upper tip toward the specimen surface. As shown in Fig. 6d, when the opening is diagonal and the joint or fault is positioned at a 30° angle at the tunnel head, lateral or tensile cracks may propagate from the tip of the joint. These cracks can extend parallel to the forcing direction along the surface of the specimen and the crown of the tunnel. In Fig. 6e, with a diagonal opening and the joint vertically aligned (at a 90-degree angle) above the tunnel head at a short distance (not interrupting the tunnel), tensile cracks propagate from both sides of the joint tip and propagate directly. Fig. 6f depicts a scenario where the opening is positioned diagonally (with the notch at a 120-degree angle), and the joint is located at an angle above the tunnel. In this case, tensile cracks originate from both ends of the joint and extend toward the top of the opening surface of the sample.

Calibrating the uniaxial compressive strength model for numerical simulation

The properties of the concrete-gypsum layered specimens were calibrated for the ABAQUS software version 6.13, and the parameters are mentioned in Table 6. In the uniaxial compressive strength test, the loading of the model was at 0.001 mm/s (Fig. 7).

Numerical simulations

In this research, the concrete-gypsum specimens, each containing a tunnel and a joint, were implicitly simulated using the XFEM. In the XFEM, the crack is represented as an enrichment zone and integrated with the traditional finite element method using the partition of unity approach [35]. The XFEM is used to model the breakage mechanism and analyze cracks in tested specimens of brittle materials. Numerical simulations of rectangular blocks under compression tests are carried out using the ABAQUS software.

Numerical modeling using the XFEM approach

The FEM is used to model the mechanism of self-induced cracking and failure in solid mechanics using the XFEM. This method utilizes enriched elements to diminish the influence of the singularity of the crack tip on stress concentration in critical areas of concrete. This version uses an independent formulation and treatment of the affected surfaces near the crack tip, ignoring the need to re-mesh the model after the crack propagation step, as is the operation required in FEM. Initial finite element mesh divides the entire problem domain into smaller elements, consisting of the existing flaws. Also, the load is gradually used to the structure. Near the crack tips, the fracture process zone is discretized with enriched elements, allowing for crack propagation.

In this modeling, integral J is used based on the method to forecast the strain energy release rate per unit of the fracture surface.

Linear path integral is not dependent on the path on every side of the crack. New experimental techniques were created to measure critical breakage characteristics with small laboratory samples for materials that do not meet the assumptions of linear elastic fracture mechanics [36]. These methods were useful particularly for materials with limited sample sizes, allowing researchers to deduce the critical value of fracture energy (J_{Ic}). Also, The J_{Ic} indicates the point at which significant plastic deformation happens during loading mode. This holds linear elastic materials at the crack tip under quasi-static conditions [37-39].

ABAQUS version 6.13 simulated the failure pattern in concrete-gypsum layers specimens with an opening containing a single joint under applied loads. To model the compression test, a cubic sample consisting of concrete-gypsum layers with a shape-opening and a single joint was developed in ABAQUS. The models were created to represent compression tests in concrete-gypsum layered specimens with various shape openings and a single joint. In constructing the numerical model, it was constrained in both side directions and positioned between two layers, as illustrated in Fig. 8 and the compressive loading velocity was 0.001 mm/s.

In this research, the same as in the experimental tests, six different specimens with various joints and different shape-opening inside gypsum were built, as shown in Fig. 9. The specimens had dimensions 200 mm × 200 mm × 60 mm. These modeled specimens were loaded uniaxial, and the compressive load was calculated by considering the reaction loads on the upper wall of the tunnel. The FEM sample had dimensions of 200 mm × 200 mm × 60 mm and contained a tunnel within the gypsum section, as shown in Fig. 9. The estimated results are presented in Figs. 9a to 9f, demonstrating concrete-gypsum layered specimens with various shapes of openings within the gypsum.

The estimated findings (i.e., Figs 9a to 9f) compared with the results obtained from the experimental tests (i.e., Fig 6a to Fig 6f). The comparison reveals a significant concurrence between the computer-simulated outcomes and the measurements obtained from laboratory tests conducted on real concrete specimens.

The breakage in specimens containing concrete-gypsum layers with a joint under compression loads (depicted in Fig. 10) was simulated using ABAQUS with XFEM. A rectangular specimen was generated in ABAQUS to replicate the manufactured specimens consisting of two layers of concrete and gypsum, with varying shape openings within the gypsum.

Fig. 10 shows the stress distribution in concrete-gypsum layers with an opening containing a single joint under compressive loading. In compression loading of these specimens, the tensile force was distributed at the tip of pre-existing cracks (joints). It means the tensile cracks begin from the tip of pre-existing joints (Fig. 10).

It was observed in Figs. 6 and 10 that both the numerical and experimental results depicted a similar pattern of breakage. This similarity indicates that the breakage pattern was consistent across the numerical models and experimental outcomes.

Effect of circular opening with single joint

Three other cases of specimens with a circular opening containing a single joint were also modeled for additional studies according to Fig. 11.

In Fig. 12, the crack pattern with stress distribution in concrete-gypsum layers with circular openings containing a single joint under compressive loading is shown. The blue and red outlines were associated with tensile and compressive stresses correspondingly.

In Fig. 12 a., the wing crack has propagated from the tip of the pre-existing joint and has reached each tip of the pre-existing joint (from the top to the surface of the sample and from the bottom to the crown of the tunnel).

In Fig. 12 b., the crack propagation path has grown vertically along the existing joint and reached the surface of the sample.

In Fig. 12 c., the crack initiated from the tip of the pre-existing joint and spread downwards.

Discussions

In the studies conducted, the failure modes of various rock specimens were analyzed in detail, focusing on the mechanisms of crack.

Wang and Zhou [40] provided insights into the failure processes in rocks, highlighting that the crack propagation modeling was not only effective but also aligned with experimental observations. However, an in-depth discussion on the specific failure stresses for each sample would enhance the understanding of the fracture behavior further. Zhou and Chen [41] introduced a novel geometrical technique for crack representation in rock slopes with non-persistent en-echelon joints. Their findings indicated distinct brittle failure mechanisms; however, a detailed examination of the failure stresses related to the experimental samples would provide added clarity regarding the conditions leading to these failures. Zhou et al. [42] utilized a field-enriched finite element technique to assess crack growth in brittle material. They investigated various configurations, including centrally cracked circular discs and Brazilian disk specimens. A discussion on the failure stresses observed in these tests could reveal significant correlations with the reported crack growth behaviors. Chen et al. [43] improved the representation of crack propagation by combining a new geometric technique with a piecewise linear function in the XFEM. Their results demonstrated increased accuracy and stability; however, an analysis of the failure stresses for the numerically simulated samples would provide valuable comparisons with the experimental results.

Additionally, Table 8 lists the outcomes of failure stress and crack initiation stress for all six experimental specimens. The data show that crack initiation and failure stress are nearly equal and that crack growth begins simultaneously with the application of stress. A comprehensive discussion addressing the implications of these failure stresses across the different study samples is essential.

The commonly recognized problem of a central slant crack in an infinite medium was chosen to evaluate the accuracy and applicability of the ABAQUS software. This decision was based on the established analytical solutions for the mode I intensity factors. The samples include inclined central crack in an infinite medium subjected to compressive stress, considering a crack length. The analytical approach to determine the stress intensity factor for a central crack that is inclined in an infinite medium is represented by the subsequent equation:

$$K_I = \sigma\sqrt{\pi a}\omega_I \quad (1)$$

The stress intensity factors mode I are represented by K_I , respectively. In this framework, σ signifies the compressive stress, and a represents the crack's half-length. The dimensionless coefficient ω_I is dependent on α . These coefficients can be articulated in the following manner:

$$\omega_I = \frac{1 + \text{Sin}(2\alpha)}{2} \quad (2)$$

In both numerical and analytical evaluations, the normalized stress intensity factor K_I^N has been utilized.

$$K_I^N = \frac{K_I}{\sigma\sqrt{\pi a}} \quad (3)$$

The pure loading mode I occurs at $\alpha = 0^\circ$ and the mechanical characteristics examined in this research encompass compressive strength, $\sigma_c = 10$ MPa. The numerical and analytical values of the stress intensity factor (K_I^N) for a centrally inclined crack at three different angles α ($0^\circ, 45^\circ$ and 90°) are presented in Table 9.

The normalized stress intensity factor (K_I^N) close to the primary pre-joint tips has been numerically evaluated for all the models. The stress intensity factor (K_I^N) near the upper and lower crack tips of the pre-joint crack are presented in Table 10.

Conclusions

Therefore, in this article, the effect of anisotropy and opening geometry on instability and failure in layered concrete-gypsum specimens with different geometries and single joints above the opening with different angles has been investigated experimentally and numerically. Results show that:

- Tensile cracks are the dominant mode of cracks that occurred in these specimens.
- In all specimens, several shear bars cut the opening space.
- When the joints are in the position connected to the opening, wing cracks start at the tip of the joint and propagate and coalesce perpendicular to the loading surface.
- When the joint is in the position connected to the tunnel head, the crack starts from the tip of the joint crack and propagates almost along the axis of the joint perpendicular to the loading surface.
- When the joint aligns with the tunnel head and has a positive angle, cracks in the wing start at the joint tip and propagate vertically until reaching the tunnel head.
- By comparing the experimental and numerical results, it can be concluded that the fracture stress is almost the same for both conditions.

Funding

The author has not disclosed any funding.

Declarations of Interest

The author has no conflicts of interest to declare that is relevant to the content of this article.

References

1. Zhu, W.C., Liu, J., Tang, C.A., Zhao, X.D., Brady, B.H., “Simulation of progressive fracturing processes around underground excavations under biaxial compression”, *Tunneling and Underground Space Technology Journal*, 20(3), p. 231-247, (2005), <https://doi.org/10.1016/j.tust.2004.08.008>
2. Zhou, X.P., Xia, E.M., Yang, H.Q., Qian, Q.H., “Different crack sizes analyzed for surrounding rock mass around underground caverns in Jinping I hydropower station”, *Theoretical and Applied Fracture Mechanics*, 57(1), p. 19-30, (2012), <https://doi.org/10.1016/j.tafmec.2011.12.004>

3. Zhu, W.C., "Simulating excavation damaged zone around a circular opening under hydro mechanical conditions", *International Journal of Rock Mechanics and Mining Sciences*, 45, p. 815-830, (2008), <https://doi.org/10.1016/j.ijrmms.2007.09.007>
4. Behzad, M., Ebrahimi, A., Meghdari, A., "A continuous vibration theory for beams with a vertical edge crack", *Scientia Iranica, Transactions B: Mechanical Engineering*, 17(3), p. 194-204, (2010), http://scientiairanica.sharif.edu/article_3290.html
5. Gratchev, I., Kim, D.H., Chong, K.Y., "Strength of rock-like specimens with pre-existing cracks of different length and width", *Rock Mechanics and Rock Engineering*, 49(11), (2016), <https://doi.org/10.1007/s00603-016-1013-1>
6. Mastali, M., Mastali, M., Abdollahnejad, Z., Dalvand, A., "Increasing the flexural capacity of geopolymers concrete beams using partial deflection hardening cement-based layers: A numerical study", *Scientia Iranica, Transactions A: Civil Engineering*, 24(6), (2017), p. 2832-2844, <https://doi.org/10.24200/sci.2017.4530>
7. Cao, R.H., Cao, P., "Mechanical behavior of an opening in a jointed rock-like specimen under uniaxial loading: Experimental studies and particle mechanics approach", *Archives of Civil and Mechanical Engineering*, 18, p. 198-214, (2018), <https://doi.org/10.1016/j.acme.2017.06.010>
8. Bagher Shemirani, A., Lawaf, M.P., "Prediction of tensile strength of concrete using the machine learning methods", *Asian Journal of Civil Engineering*, 25, p. 1207-1223, (2023), <https://doi.org/10.1007/s42107-023-00837-5>
9. Zhao, X., "Automated rotational- and scaling-invariant image-based crack width monitoring with sub-millimeter accuracy and self-numbering label", 21, p. 741-749, (2020), <https://doi.org/10.1007/s42107-020-00235-1>
10. Bagher Shemirani, A., "Experimental and numerical studies of concrete bridge decks using ultra high-performance concrete and reinforced concrete", *Computers and Concrete*, 29(6), p. 407-418, (2022), <https://doi.org/10.12989/cac.2022.29.6.407>
11. Fahimi, S., Zakerzadeh, M.R., Baghani, M., Zandi, K., "A novel method for implementation of corrosion-induced cracks in the finite element models of reinforced concrete structures", *Scientia Iranica, Transactions A: Civil Engineering*, 28(3), p. 1079-1095, (2021), <https://doi.org/10.24200/sci.2020.52829.2903>
12. Bagher Shemirani, A., "Effects of fiber combination on the fracture resistance of hybrid reinforced concrete", *Iranian Journal of Science and Technology, Transactions of Civil Engineering*, 46, p. 2161-2172, (2022), <https://doi.org/10.1007/s40996-021-00703-x>
13. Badrikouhi, E., Adibnazari, S., "A new model for predicting fretting fatigue crack initiation life based on effective slip amplitude", *Scientia Iranica, Transactions B: Mechanical Engineering*, 30(4), p. 1255-1264, (2023), <https://doi.org/10.24200/sci.2022.60534.6849>
14. Bagher Shemirani, A., "Prediction of fracture toughness of concrete using the machine learning approach", *Theoretical and Applied Fracture Mechanics*, 134(B), 104749, (2024), <https://doi.org/10.1016/j.tafmec.2024.104749>
15. Li, J., Wang, Z.F., Wang, Y., Chang, H.t., "Analysis and countermeasures of large deformation of deep-buried tunnel excavated in layered rock strata: a case study", *Engineering Failure Analysis*, 146, 107057, (2023), <https://doi.org/10.1016/j.engfailanal.2023.107057>
16. Sun, B.j., Mei, Y.C., Li, W.T., Zhang, C., Shao, X., Li, T.C., Li, W.X., Zhao, W.X., Wang, L.p., "Experimental study on the deformation and failure mode of surrounding rocks of a tunnel in a jointed rock mass", *Engineering Failure Analysis*, 163(Part A), 108470, (2024), <https://doi.org/10.1016/j.engfailanal.2024.108470>

17. Si, X., Luo, Y., Luo, S., “Influence of lithology and bedding orientation on failure behavior of “D” shaped tunnel”, *Theoretical and Applied Fracture Mechanics*, 129, 104219, (2024), <https://doi.org/10.1016/j.tafmec.2023.104219>
18. Deng, Z., Zhu, Z., Zhou, L., Ma, L., Huang, J., Zhang, Y., “Effect of dynamic loading orientation on fracture properties of surrounding rocks in twin tunnels”, *Journal of Rock Mechanics and Geotechnical Engineering*, 16 (2), p.393-409, (2024), <https://doi.org/10.1016/j.jrmge.2023.06.017>
19. Chen, Z., Yao, Y., Wang, B., Xie, Q., Zhou, Z., Jiang, C., “Stability analysis and failure mechanism of multiple parallel soft-rock tunnels considering the random distribution of rock mass joints”, *Engineering Failure Analysis*, 159, 108150, (2024), <https://doi.org/10.1016/j.engfailanal.2024.108150>
20. Li, Y., Yuan, L., Zhang, Q., “Brittle rock mass failure in deep tunnels: the role of infilled structural plane with varying dip angles”, *International Journal of Rock Mechanics and Mining Sciences*, 176, 105721, (2024), <https://doi.org/10.1016/j.ijrmms.2024.105721>
21. Huang, J., Song, Y., Lei, M., Shi, C., Jia, C., Zhang, J., “Numerical study on the damage characteristics of layered shale using 3D DEM”, *KSCE Journal of Civil Engineering*, 27, p. 5436-5447, (2023), <https://doi.org/10.1007/s12205-023-0411-7>
22. Chen, Y., Teng, J., “3DEC numerical analysis of failure characteristics for tunnel in stratified rock masses”, *KSCE Journal of Civil Engineering*, 28, p. 2420-2426, (2024), <https://doi.org/10.1007/s12205-024-1318-7>
23. He, M., Zhao, J., Deng, B., Zhiqiang, Z., “Effect of layered joints on rock burst in deep tunnels”, *International Journal of Coal Science & Technology*, 9(21), (2022), <https://doi.org/10.1007/s40789-022-00489-x>
24. Zhou, X.P., Yang, H.Q., “Multiscale numerical modeling of propagation and coalescence of multiple cracks in rock masses”, *International Journal of Rock Mechanics and Mining Sciences*, 55, p. 15-27, ISSN 1365-1609, (2012), <https://doi.org/10.1016/j.ijrmms.2012.06.001>
25. Chen, J., Gu, S., Zhou, X., “The effects of weak interlayers on the dynamic mechanical properties and failure behaviours of rocks: a combined numerical and experimental analysis”, *International Journal of Impact Engineering*, 180, 104680, ISSN 0734-743X, (2023), <https://doi.org/10.1016/j.ijimpeng.2023.104680>
26. Chen, J., Zhou, X., “An investigation on the effect of crack lengths and wavelengths on the dynamic cracking behaviours of brittle materials using the improved XFEM”, *Engineering Fracture Mechanics*, 277, 109008, ISSN 0013-7944, (2023), <https://doi.org/10.1016/j.engfracmech.2022.109008>
27. Zhou, X., Jia, Z., “Dynamic propagation of moving cracks in brittle materials by field-enriched finite element method”, *Engineering Fracture Mechanics*, 305, 110177, ISSN 0013-7944, (2024), <https://doi.org/10.1016/j.engfracmech.2024.110177>
28. Chen, J., Zhou, X., Zhou, L., “The enriched degree of freedom method for the absorbing boundary and its application to XFEM in elastodynamic problems”, *Applied Mathematical Modelling*, 112, p. 168-198, ISSN 0307-904X, (2022), <https://doi.org/10.1016/j.apm.2022.08.007>
29. Zhou, X.P., Chen, J.W., Berto, F., “XFEM based node scheme for the frictional contact crack problem”, *Computers and Structures*, 231, 106221, ISSN 0045-7949, (2020), <https://doi.org/10.1016/j.compstruc.2020.106221>
30. Chen, J., Zhou, X., Zhou, L., Berto, F., “Simple and effective approach to modeling crack propagation in the framework of extended finite element method”, *Theoretical and Applied*

- Fracture Mechanics, 106, 102452, ISSN 0167-8442, (2020), <https://doi.org/10.1016/j.tafmec.2019.102452>
31. Zhou, X.P., Zhang, J.Z., Qian, Q.H., Niu, Y., “Experimental investigation of progressive cracking processes in granite under uniaxial loading using digital imaging and AE techniques”, *Journal of Structural Geology*, 126, p. 129-145, ISSN 0191-8141, (2019), <https://doi.org/10.1016/j.jsg.2019.06.003>
32. Zhou, X.P., Cheng, H., Feng, Y.F., “An experimental study of crack coalescence behaviour in rock-like materials containing multiple flaws under uniaxial compression”, *Rock Mechanics and Rock Engineering*, 47, p. 1961-1986, (2014), <https://doi.org/10.1007/s00603-013-0511-7>
33. Chen, J.W., Zhou, X.P., “The enhanced extended finite element method for the propagation of complex branched cracks”, *Engineering Analysis with Boundary Elements*, 104, p. 46-62, ISSN 0955-7997, (2019), <https://doi.org/10.1016/j.enganabound.2019.03.028>
34. Chen, J., Zhou, X., Zhou, L., Berto, F., “Simple and effective approach to modeling crack propagation in the framework of extended finite element method”, *Theoretical and Applied Fracture Mechanics*, 106, 102452, ISSN 0167-8442, (2020), <https://doi.org/10.1016/j.tafmec.2019.102452>
35. Ebrahimi, S.H., Mohammadi, S., Asadpoure, A., “An extended finite element (XFEM) approach for crack analysis in composite media”, *International Journal of Civil Engineering*, 6(3), p. 198-207, (2008), <http://ijce.iust.ac.ir/article-1-179-en.html>
36. Cherepanov, G.P., “Crack propagation in continuous media”, *Journal of Applied Mathematics and Mechanics (translation of PMM)*, 31, p. 476-488, (1967), [https://doi.org/10.1016/0021-8928\(67\)90034-2](https://doi.org/10.1016/0021-8928(67)90034-2)
37. Rice, J.R., “Stresses due to a sharp notch in a work-hardening elastic-plastic material loaded in longitudinal shear”, *Journal of Applied Mechanics*, 34, p. 287-298, (1967a), <https://doi.org/10.1115/1.3607681>
38. Rice, J.R., “The mechanics of crack tip deformation and extension by fatigue. in: fatigue crack growth”, *Special Technical Publication 415*, American Society for Testing and Materials, Philadelphia, p. 247-311, (1967b), <https://doi.org/10.1520/STP47234S>
39. Budiansky, B., Rice, J.R., “Conservation laws and energy release rates”, *Journal of Applied Mechanics*, 40, p. 201-203, (1973), <https://doi.org/10.1115/1.3422926>
40. Wang, L.F., Zhou, X.P., “A field-enriched finite element method for simulating the failure process of rocks with different defects”, *Computers and Structures*, 250, 106539, ISSN 0045-7949, (2021), <https://doi.org/10.1016/j.compstruc.2021.106539>
41. Zhou, X.P., Chen, J., “Extended finite element simulation of step-path brittle failure in rock slopes with non-persistent en-echelon joints”, *Engineering Geology*, 250, p. 65-88, ISSN 0013-7952, (2019), <https://doi.org/10.1016/j.enggeo.2019.01.012>
42. Zhou, X.P., Jia, Z., Wang, L.F., “A field-enriched finite element method for brittle fracture in rocks subjected to mixed mode loading”, *Engineering Analysis with Boundary Elements*, 129, p. 105-124, ISSN 0955-7997, (2021), <https://doi.org/10.1016/j.enganabound.2021.04.023>
43. Chen, J.W., Zhou, X.P., Berto, F., “The improvement of crack propagation modelling in triangular 2D structures using the extended finite element method”, *Fatigue and Fracture of Engineering Materials and Structures*, 42(2), p. 397-414, (2018), <https://doi.org/10.1111/ffe.12918>

Caption of figures

Fig. 1. Custom-designed wooden containers used for creating concrete-gypsum layers

Fig. 2. Concrete-gypsum layers with a joint

Fig. 3. Testing setup

Fig. 4. The geometries show openings with different angles of joints.

Fig. 5. The fabricated specimens from two concrete-gypsum layers with a joint

Fig. 6. Failure pattern of concrete-gypsum layers with opening containing single joint

Fig. 7. The numerical models a) concrete sample failure and b) gypsum sample failure.

Fig. 8. Building a numerical model with XFEM

Fig. 9. Concrete-gypsum layer specimens with openings containing single joints

Fig. 10. Numerical simulation of failure pattern in concrete-gypsum specimens with opening containing single joint

Fig. 11. Three other cases of specimens with a circular opening containing a single joint were also modeled for additional studies.

Fig. 12. The crack pattern with stress distribution in concrete-gypsum layers'

Caption of tables

Table 1. Cement and silica fume properties for the admixture

Table 2. Physical aggregates properties

Table 3. Details of materials used to make concrete specimens

Table 4. Mechanical characteristics of gypsum specimens

Table 5. Mechanical characteristics of concrete specimens

Table 6. Parameters of concrete-gypsum layered specimens using XFEM

Table 7. Uniaxial compressive strengths of the concrete/gypsum specimens without opening and joint were obtained experimentally and simulated numerically by ABAQUS.

Table 8. Crack initiation stress and final stress for all six experimental specimens

Table 9. The numerical and analytical values of the stress intensity factors (K_I^N)

Table 10. The stress intensity factor (K_I^N)

Figures:



Fig. 1. Custom-designed wooden containers used for creating concrete-gypsum layers



Fig. 2. Concrete-gypsum layers with a joint



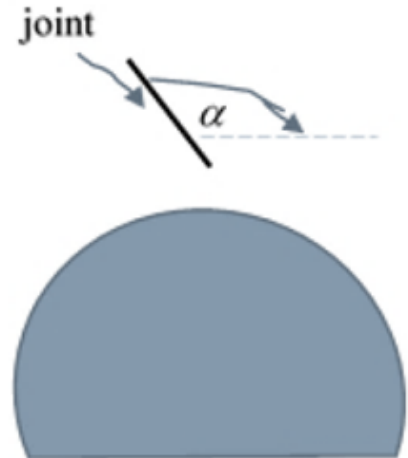
Fig. 3. Testing setup



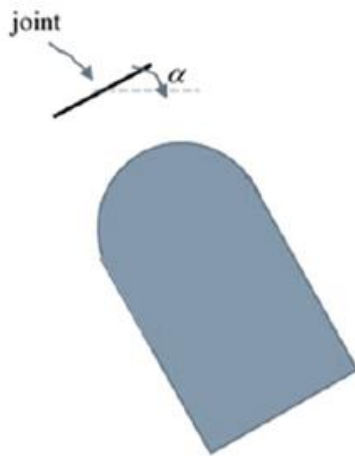
(a)



(b)



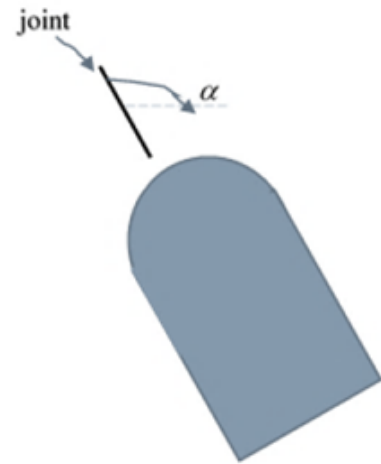
(c)



(d)



(e)



(f)

Fig. 4. The geometries show openings with different angles of joints, a) $\alpha = 45^\circ$, b) $\alpha = 90^\circ$, c) $\alpha = 125^\circ$, d) $\alpha = 30^\circ$, e) $\alpha = 90^\circ$, f) $\alpha = 120^\circ$

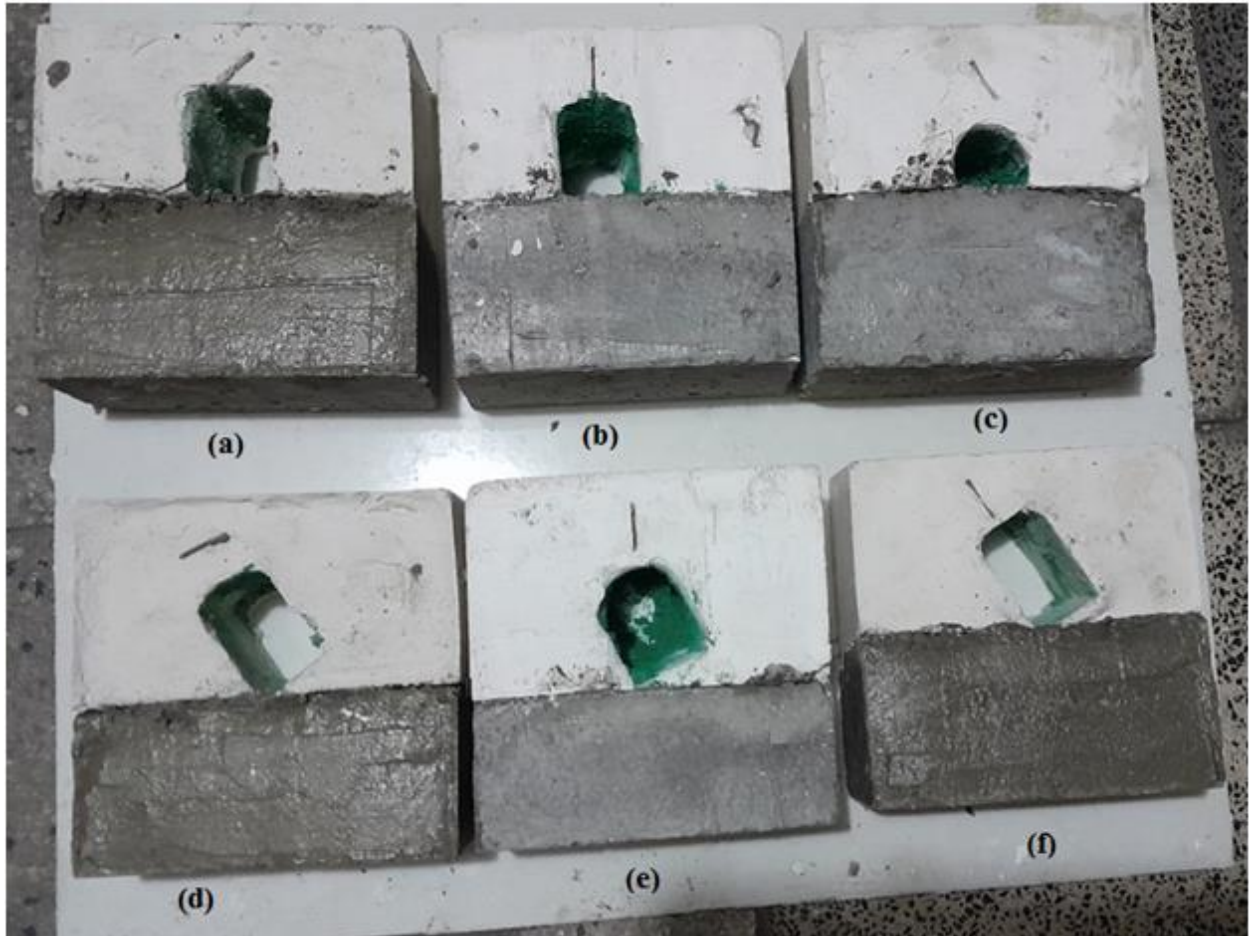


Fig. 5. The fabricated specimens from two concrete-gypsum layers with a joint

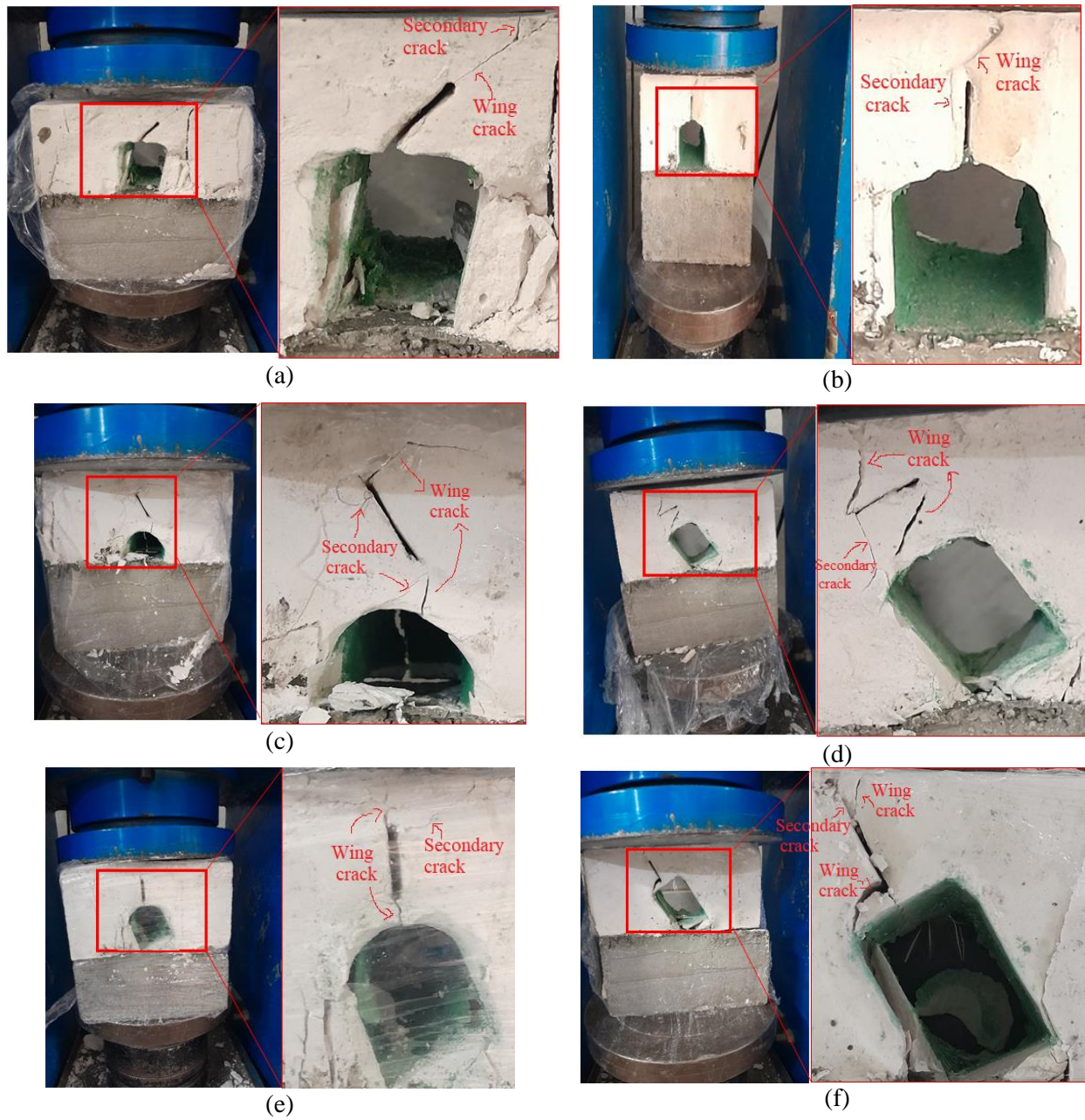


Fig. 6. Failure pattern of concrete-gypsum layers with opening containing single joint

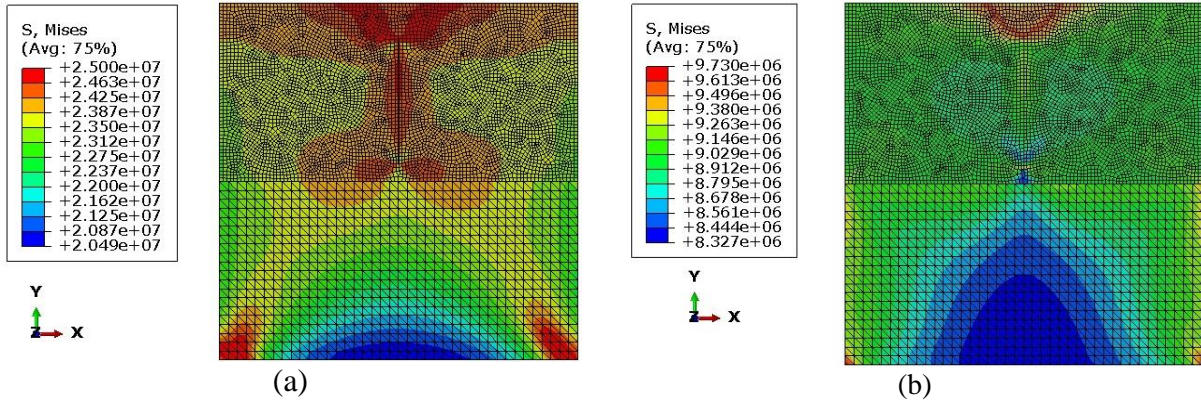


Fig. 7. The numerical models a) concrete sample failure and b) gypsum sample failure

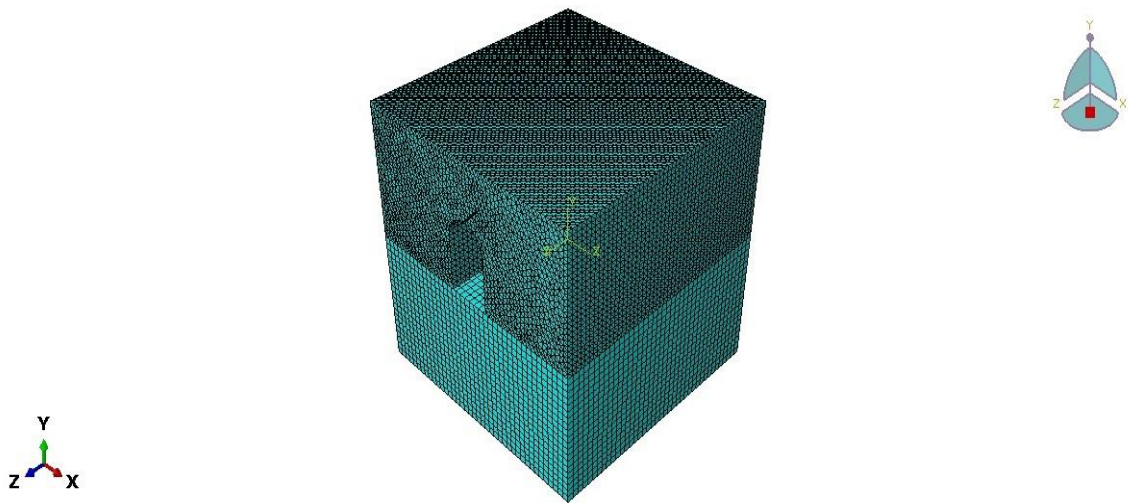
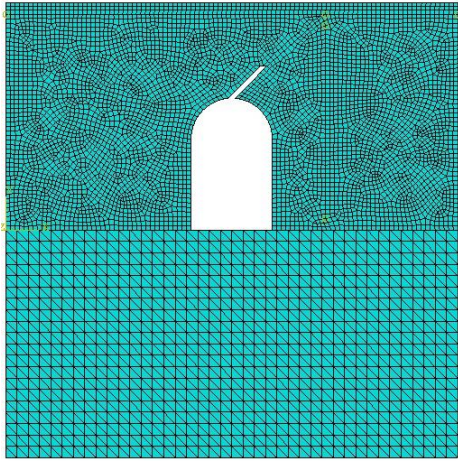
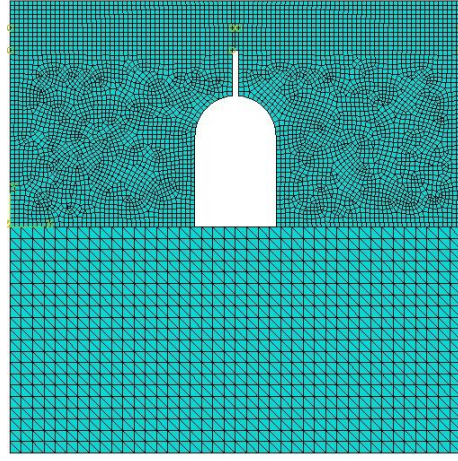


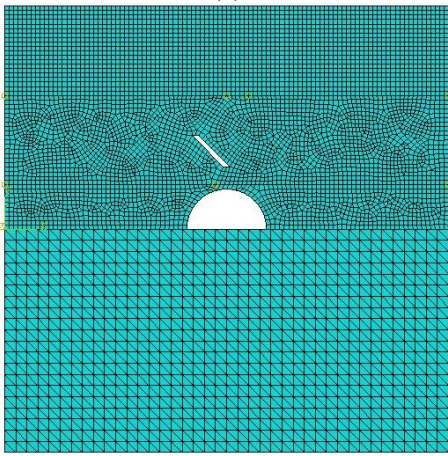
Fig. 8. Building a numerical model with XFEM



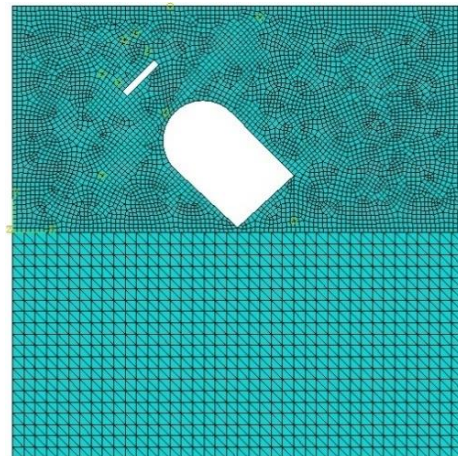
(a)



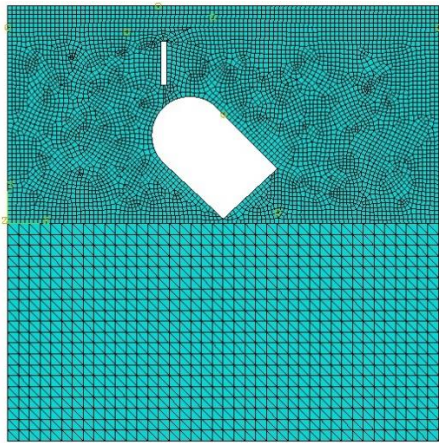
(b)



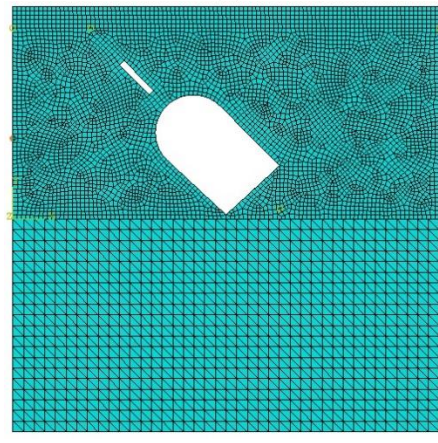
(c)



(d)



(e)



(f)

Fig. 9. Concrete-gypsum layer specimens with openings containing single joints

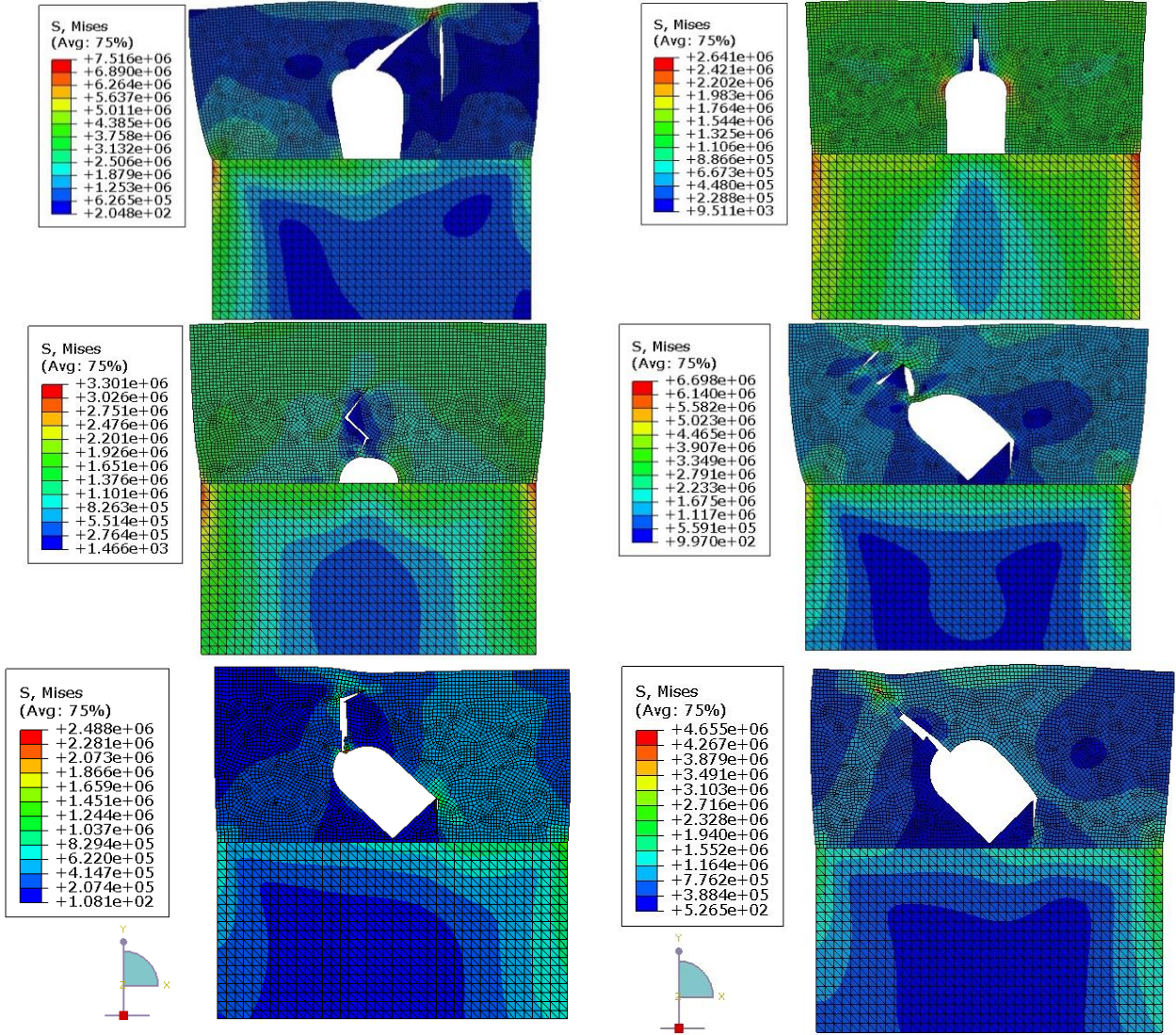


Fig 10. Numerical simulation of failure pattern in concrete-gypsum specimens with opening containing single joint

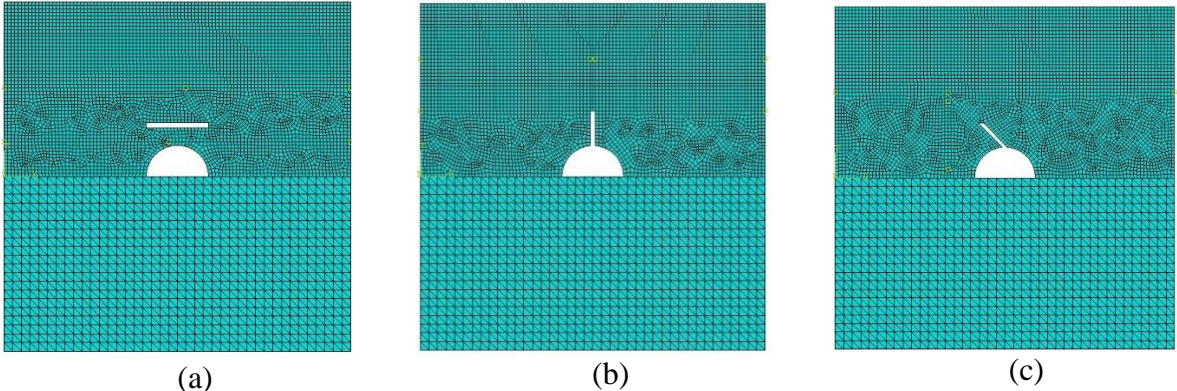
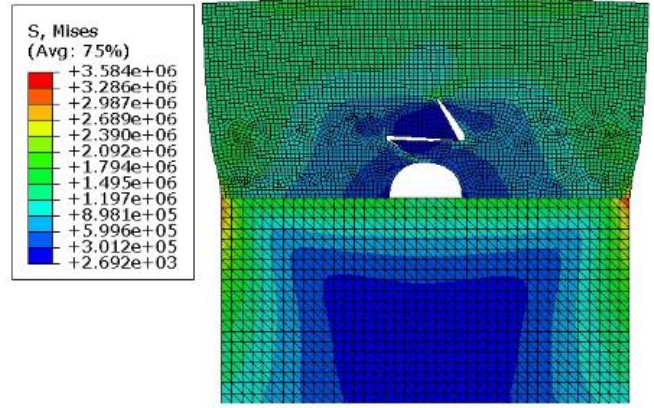
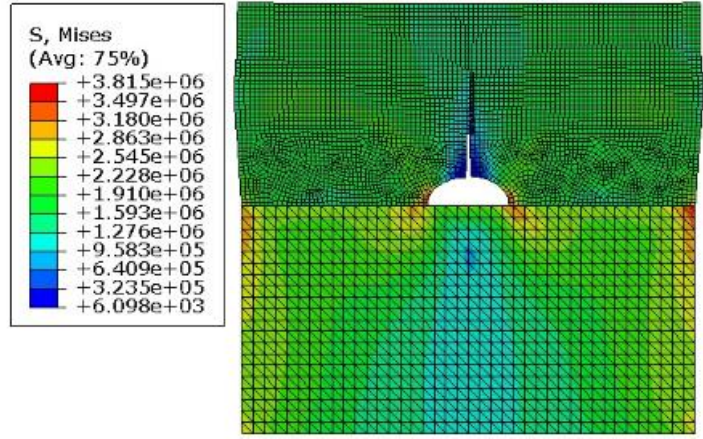


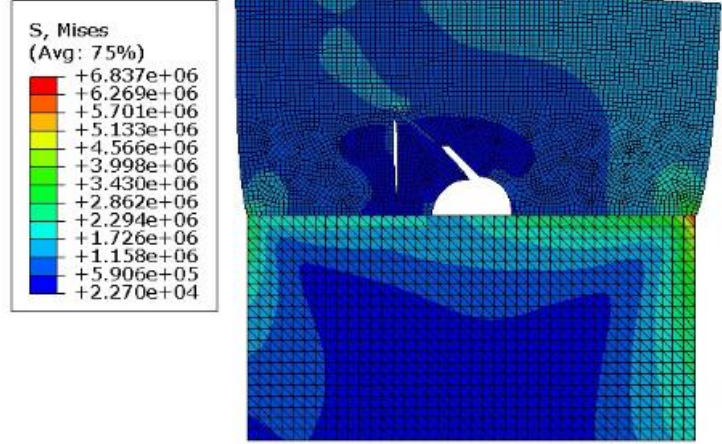
Fig. 11. Three other cases of specimens with a circular opening containing a single joint were also modeled for additional studies



(a)



(b)



(c)

Fig. 12. The crack pattern with stress distribution in concrete-gypsum layers'

Tables:

Table 1. Cement and silica fume properties for the admixture

Properties	Physical properties	
	Cement	Silica fume
Specific gravity (gr/cm ³)	3.15	2.20
Bulk density (kg/m ³)	-	576
Initial setting time (min)	45	-
Final setting time (min)	375	-
	Chemical properties	
SiO ₂ (%)	90-96	20-25
Al ₂ O ₃ (%)	0.5-0.8	4-8

Table 2. Physical aggregates properties

Index	Value
Specific gravity (gr/cm ³)	2.63
Passing 4.75-mm sieve (%)	100
Maximum dry density (kN/m ³)	15.5
Minimum dry density (kN/m ³)	12.3
D ₁₀ (mm)	0.194
D ₅₀ (mm)	0.322
D ₆₀ (mm)	0.344

Table 3. Details of materials used to make concrete specimens

Material	Portland Cement	Silica fume	Water	Fine aggregate (sand)	Coarse aggregate (gravel)	Super-plasticizer
Density (kg/m ³)	450	20	180	850	840	6

Table 4. Mechanical characteristics of gypsum specimens

Mechanical properties	Experimental results
Elastic modulus, (GPa)	15
Poisson's ratio	0.18
Uniaxial compressive strength (MPa)	10
Splitting tensile strength (MPa)	1

Table 5. Mechanical characteristics of concrete specimens

Mechanical properties	Experimental results
Elastic modulus, (GPa)	23.5
Poisson's ratio	0.2
Uniaxial compressive strength, (MPa)	25
Splitting tensile strength (MPa)	4

Table 6. Parameters of concrete-gypsum layered specimens using XFEM

Young modulus (GPa)	Poisson's ratio	Density (kg/m ³)	Compressive Strength (MPa)	MAXPS Damage (MPa)	GI (N/m)
23.5	0.2	2400	25	3.5	250

Table 7. Uniaxial compressive strengths of the concrete/gypsum specimens without opening and joint were obtained experimentally and simulated numerically by ABAQUS.

Uniaxial compression strength	Experimental	Numerical
Compression strength of gypsum (MPa)	10	9.73
Compression strength of concrete (MPa)	25	25

Table 8. Crack initiation stress and final stress for all six experimental specimens



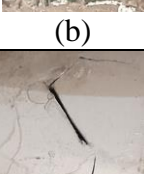
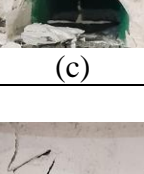

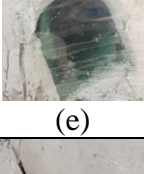
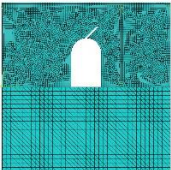
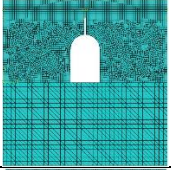
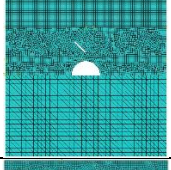
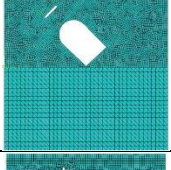
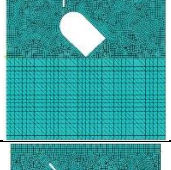
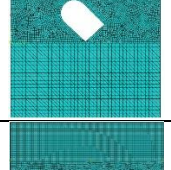
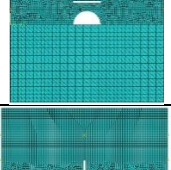
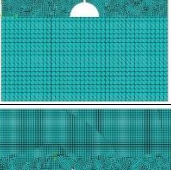
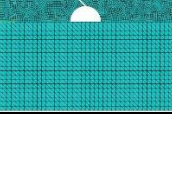
Different models	Experimental	Numerical
 (a)	Crack initiation stress=6.9 MPa Final tensile stress=7.4 MPa	Crack initiation stress=6.3 MPa Final tensile stress=7.5 MPa
 (b)	Crack initiation stress=2.1 MPa Final tensile stress=2.4 MPa	Crack initiation stress=2.2 MPa Final tensile stress=2.6 MPa
 (c)	Crack initiation stress=2.6 MPa Final tensile stress= 3.3 MPa	Crack initiation stress=2.8 MPa Final tensile stress=3.3 MPa
 (d)	Crack initiation stress=6.0 MPa Final tensile stress= 6.5 MPa	Crack initiation stress= 5.6 MPa Final tensile stress= 6.7 MPa
 (e)	Crack initiation stress=2.2 MPa Final tensile stress= 2.4 MPa	Crack initiation stress= 2.1 MPa Final tensile stress= 2.5 MPa
 (f)	Crack initiation stress=3.6 MPa Final tensile stress= 4.5 MPa	Crack initiation stress= 3.9 MPa Final tensile stress= 4.7 MPa

Table 9. The numerical and analytical values of the stress intensity factors (K_I^N)

$\alpha^{(\circ)}$	K_I^N	
	Numerical	Analytical
0	0.005	0
45	0.512	0.5
90	1.12	1

Table 10. The stress intensity factor (K_I^N)

Simulated samples	K_I^N	
	Upper Crack	Lower Crack
	0.510	-
	1.015	-
	0.693	0.699
	0.282	0.286
	1.033	1.039
	0.599	0.600
	0.0015	0.0017
	1.009	1.010
	0.675	-

Biographies

Dr. Alireza Bagher Shemirani received his Ph.D. in Civil Engineering from The Sharif University of Technology in 2016, under the supervision of Professor R. Naghdabadi from The Sharif University of Technology. He is currently an assistant professor in the Civil, Water & Environmental Engineering Department at Shahid Beheshti University. His research interests include concrete materials, crack propagation, and computational mechanics.